

# Direct evidence of open ray orbits in a square two-dimensional resonator of dye-doped polymers

G. D. Chern, A. W. Poon,\* and R. K. Chang

*Department of Applied Physics, Yale University, New Haven, Connecticut 06520*

T. Ben-Messaoud, O. Alloschery, E. Toussaere, and J. Zyss

*École Normale Supérieure de Cachan, 94235 Cachan, Cedex, France*

S.-Y. Kuo

*National Chiao Tung University, Hsinchu, Taiwan 30050, China*

Received February 6, 2004

Lasing has been observed in optically pumped 4-dicyanomethylene-2-methyl-6-(*p*-dimethylamino-styryl)-4*H*-pyran-doped poly(methyl methacrylate) square-shaped micropillars that allow four-bounce closed and open ray orbits with internal incident angle  $\theta_{\text{inc}} > \theta_c$  (the critical angle for total internal reflection) and with the associated surface waves that emit at the four corners. We also detect strongly TE-polarized and spatially varying emission from the square sidewalls that is due to leaky open ray orbits with  $\theta_{\text{inc}}$  near but less than  $\theta_c$  for two of the four bounces. By selectively pumping the square microcavity with a stripe-shaped beam, we excite different four-bounce ray orbits. © 2004 Optical Society of America

OCIS codes: 230.3990, 230.5750.

Two-dimensional microcavities are enjoying interest for their potential applications, e.g., microdisk lasers for integrated optoelectronic devices<sup>1</sup> and compact optical channel add-drop filters for wavelength-division multiplexing.<sup>2</sup> In the latter case, a micro-ring resonator is placed close to two optical waveguides such that their external evanescent fields overlap. The coupling ratio depends on the coupling length between the ring and the waveguide, which is pointlike and therefore gives a small coupling ratio. To overcome this shortcoming, a submicrometer separation between the ring and the waveguides is required and complicates fabrication.<sup>2</sup>

A square-shaped microcavity<sup>3</sup> has been proposed as an alternative to the micro-ring. For a square resonator the coupling length could be the entire square sidewall, thereby greatly lengthening the coupling distance and relaxing the need for submicrometer fabrication. Unlike square ring lasers, these square microcavities do not require additional total internal reflection (TIR) mirrors at the corners<sup>4</sup> because TIR occurs off the four sidewalls of the square microcavity.

Another advantage of the square resonator is its closed ray orbits, which have the following properties: (1) rays return to their initial positions after only four bounces, (2) every reflection has an internal incident angle  $\theta_{\text{inc}} = 45^\circ$ , and (3) more importantly, all closed ray orbits have the same path length, independently of their initial positions. Because  $\theta_{\text{inc}} > \theta_c$  (where  $\theta_c$  is the critical angle for TIR), resonant evanescent coupling is allowed at any position along the sidewall when discrete wavelengths are commensurate with  $\theta_{\text{inc}} = 45^\circ$  closed ray orbits. Spectral measurements of emission from the four square corners show resonances with free spectral

ranges (FSRs) in good agreement with those that correspond to closed ray orbits.

Open ray orbits, where  $\theta_{\text{inc}} \neq 45^\circ$ , can also exist within the square resonator and be TIR confined if  $\theta_{\text{inc}} > \theta_c$  for all four bounces. Nearly TIR-confined open ray orbits occur if two of the four bounces have  $\theta_{\text{inc}}$  near but less than  $\theta_c$  and are therefore leaky. These open ray orbits may be of interest particularly when one is considering square resonator filters. More generally, square cavity orbits have legs with only two possible directions (determined by  $\theta_{\text{inc}}$  and its complementary angle  $90^\circ - \theta_{\text{inc}}$ ) and a set path once  $\theta_{\text{inc}}$  and the starting position are known.

In this Letter we report the observation of TE emission (**E** field parallel to the microcavity plane) emerging with spatial variation (with  $\sim 3$  times greater intensity than corner emission) from along the entire square sidewall and confined to a limited angular range. TM emission was suppressed. We attribute the sidewall emission to nearly TIR-confined open ray orbits. The origin of this emission was further investigated with a stripe-shaped pump beam that can be angle tuned relative to the micropillar sidewalls and thereby facilitate some overlap between the pump and a particular nearly TIR-confined open ray orbit. Intensity variations along the sidewall were also observed and may be due to interference among different open ray orbits and sidewall roughnesses.

We fabricate the poly(methyl methacrylate)-4-dicyanomethylene-methyl-6-(*p*-dimethylaminostyryl)-4*H*-pyran (PMMA:DCM) micropillars (refractive index  $n = 1.49$ ) by spin coating a spin-on-glass (SOG) buffer layer onto a silicon substrate [Fig. 1(a)]. The active layer (PMMA:DCM) is then spun coated over the buffer layer and annealed in an oven at

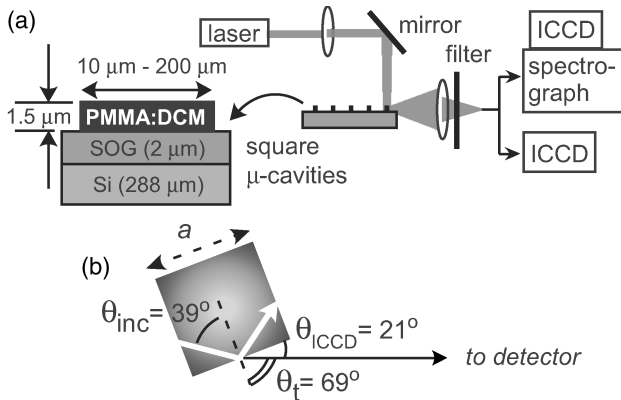


Fig. 1. (a) Setup for optical pumping. Emission from a microcavity imaged onto an intensified charge-coupled device (ICCD) camera (spectrograph) for an image (spectral) profile. Inset, PMMA:DCM sample layers. (b) Diagram of angles  $\theta_{inc}$ ,  $\theta_t$ , and  $\theta_{ICCD}$ .

120 °C. Finally, a series of microlithography and O<sub>2</sub> reactive ion etching steps creates the microcavities.

The square micropillars are optically pumped by the second harmonic ( $\lambda_p = 532$  nm) of a 100-ps Nd:YAG laser incident normally onto the top face of the micropillar [Fig. 1(a)]. The sample is uniformly exposed to the pump beam with a diameter ( $\approx 300$   $\mu\text{m}$ ) that is slightly larger than the microcavity (hereafter referred to as flood pumping). To probe the effects of selective pumping we use a cylindrical lens to produce a stripe-shaped ( $\approx 500$   $\mu\text{m} \times 30$   $\mu\text{m}$ ) pump beam. A camera lens (5° acceptance angle), which images the spatial variation of the emission and (or) the spectra from along the micropillar sidewall [Fig. 1(a)], in combination with an ICCD camera, enables us to determine from where along the sidewall the emission is emerging. Figure 1(b) diagrams the camera angle,  $\theta_{ICCD}$ . With the insertion of an imaging spectrograph, the emission spectrum from the corners and along the sidewalls is also spatially resolved. A 590-nm long-pass filter in front of the ICCD camera or spectrograph blocks the 532-nm pump light.

From square micropillars, we achieved directional (along the sidewalls) laser emission from the corners (Fig. 2, inset). We confirmed lasing by observing nonlinear dependence of the output intensity on the input power, and spectral narrowing. The emission is attributed to closed ray orbits that have all rays with  $\theta_{inc} = 45^\circ$  and thereby satisfy the TIR condition  $\theta_{inc} > \theta_c$ , where  $\theta_c = \sin^{-1}(1/n) = 42^\circ$  for PMMA. At each TIR an evanescent wave normal to the interface and a surface wave along the interface are formed. At the square corner the surface wave encounters a dielectric discontinuity and becomes a propagating wave.<sup>5</sup>

Figures 2(a) and 2(b) show the spectra of the surface-wave emission from the corners of squares of side lengths  $a = 100$  and  $a = 150$   $\mu\text{m}$ , respectively, with measured FSRs of  $\Delta\lambda = 0.80 \pm 0.04$  nm ( $a = 100$   $\mu\text{m}$ ) and  $0.54 \pm 0.02$  nm ( $a = 150$   $\mu\text{m}$ ). For comparison, the FSR can be calculated by use of the interference condition  $m\lambda = nL$ , where  $m$  is an integer,  $\lambda$  is the wavelength, and  $L = 2\sqrt{2}a$  is the closed

ray orbit path length in a square of side length  $a$ . The FSR  $\Delta\lambda$  is then given by  $\Delta\lambda = \lambda^2/(n2\sqrt{2}a)$ . The measured FSR is in excellent agreement with the calculated FSR of the closed ray orbit modes  $\Delta\lambda = 0.86 \pm 0.01$  nm ( $a = 100$   $\mu\text{m}$ ) and  $0.57 \pm 0.01$  nm ( $a = 150$   $\mu\text{m}$ ). For the 100- $\mu\text{m}$  square the measured quality factor is  $Q > 10^3$ . For larger squares, the higher- $Q$ -value modes cannot be measured because of limited spectrograph resolution.

Interestingly, the imaging technique revealed that the far-field emission peaks at a camera angle  $\theta_{ICCD} = 21^\circ$  [Fig. 3(a)] instead of at  $\theta_{ICCD} = 0^\circ$ , which corresponds to corner emission. Here  $\theta_{ICCD} = 90^\circ - \theta_t$ , where  $\theta_t$  is the transmission angle in air as determined by Snell's law,  $\sin \theta_t = n \sin \theta_{inc}$  [Fig. 1(b)]. The intensity at this peak angle is three times larger than the surface-wave emission from the corners. We attribute the observed sidewall emission to escaped refractive emission of nearly TIR-confined open ray orbits. The restricted far-field angular range is a result of two factors: (1) a sufficiently large Fresnel transmission coefficient for a given  $\theta_{inc}$  and (2) a Fresnel reflection coefficient that is zero at the Brewster angle,  $\theta_B = 34^\circ$  (for PMMA:DCM).

Figure 3(b) shows several spatial peaks that come from different sidewall positions at  $\theta_{ICCD} = 21^\circ$  ( $\theta_t = 69^\circ$ ) for TE polarization. TM emission is highly suppressed. The spatial variations along the sidewall may be explained as being due to the interference of two or more open ray orbits as well as to sidewall roughness that results from the etching process.

We further characterized the sidewall emission by selectively pumping the square microcavity with a

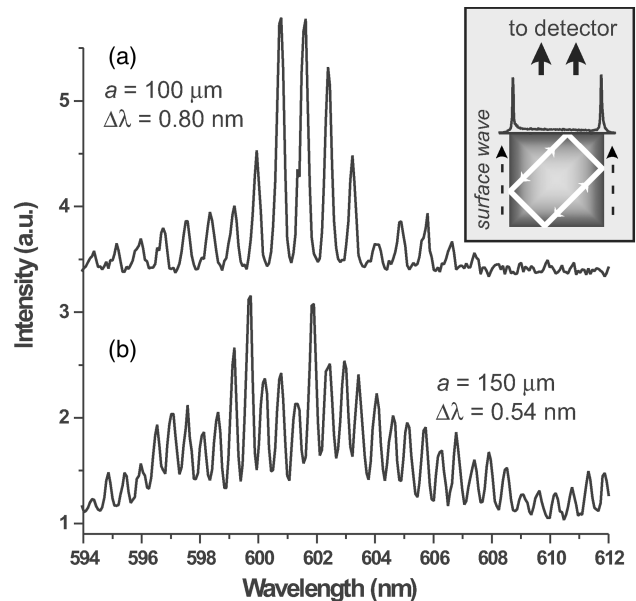


Fig. 2. Corner emission spectra of (a) 100- and (b) 150- $\mu\text{m}$  squares. FSRs  $\Delta\lambda = 0.80 \pm 0.04$  nm ( $a = 100$   $\mu\text{m}$ ) and  $\Delta\lambda = 0.54 \pm 0.02$  nm ( $a = 150$   $\mu\text{m}$ ) agree well with closed ray orbits. The  $Q$  factor for a 100- $\mu\text{m}$  square is  $Q > 10^3$ . The  $Q$  value of the larger square cannot be measured because of limited spectrometer resolution. Inset, square with a closed ray orbit relative to the ICCD.

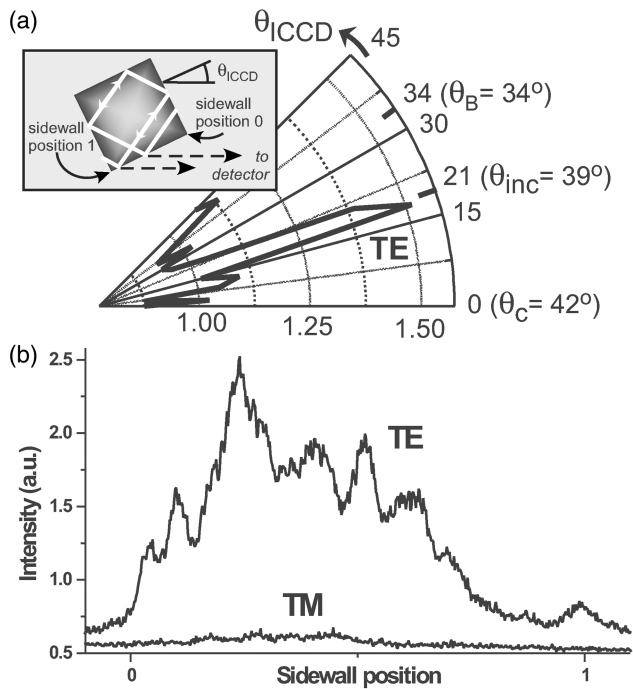


Fig. 3. (a) Far-field pattern of the  $a = 244\text{-}\mu\text{m}$  square, showing refractive emission from sidewalls peaked at  $\theta_{\text{ICCD}} \approx 21^\circ$ . The intensity decreases as  $\theta_{\text{ICCD}}$  approaches  $\theta_B = 34^\circ$ . Inset, square with open ray orbit ( $\theta_{\text{inc}} \neq 45^\circ$ ), relative to the ICCD. (b) Image profile at  $\theta_{\text{ICCD}} = 21^\circ$ . Discrete spatial emission peaks from various sidewall positions for TE polarization. TM emission is highly suppressed.

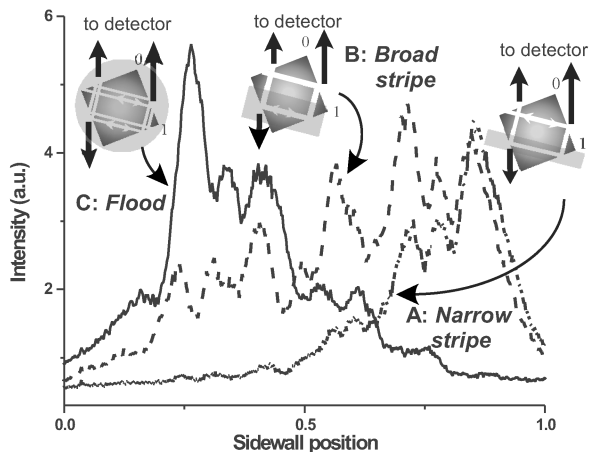


Fig. 4. Image profile at  $\theta_{\text{ICCD}} = 21^\circ$  of the  $a = 244\text{-}\mu\text{m}$  square, showing sidewall emission when the square is selectively pumped by linear beams of various widths (A, dotted and B, dashed curves) and flood pumped (C, solid curve). Intensity modulation extends throughout the sidewall as the pump beam's width increases. The orientation of the square with a laser beam, denoted by the shaded areas, selectively pumping the  $\theta_{\text{inc}} = 39^\circ$  ray trajectories shown.

stripe-shaped beam. Figure 4 shows an image profile of one sidewall, also at  $\theta_{\text{ICCD}} = 21^\circ$ , with narrow-stripe selective pumping (Fig. 4, case A). The length of

the pump beam is oriented such that rays with  $\theta_{\text{inc}} = 39^\circ$  ( $\theta_t = 69^\circ$ ,  $\theta_{\text{ICCD}} = 21^\circ$ ) just below  $\theta_c = 42^\circ$  are excited. Emission is observed only from the lower quarter of the sidewall. Widening the stripe-shaped pump beam (Fig. 4, case B) extends emission throughout the sidewall. This result can be interpreted by nearly TIR confined open ray orbits that close upon themselves not after one round trip but after many round trips. As the pump beam's width increases, there is greater spatial overlap of the pump with the excited trajectory, thereby extending the emission throughout the sidewall. Figure 4, case C, shows the flood-pumping case in which every orbit is equally pumped and escaped refractive emission is confined mainly to the top half of the sidewall.

We also measured, all in one laser firing, the emission spectra of all the different intensity peaks along the sidewall (data not shown). As expected, the resonance wavelengths of the various spatial locations are not the same, indicating that sidewall emission is not a single-mode phenomenon.

To summarize, we expected and observed directional lasing from the square micropillar corners to be consistent with the surface wave that is associated with all the equal-perimeter closed ray orbits with  $\theta_{\text{inc}} = 45^\circ$  and TIR-confined open ray orbits with  $\theta_{\text{inc}} \geq \theta_c$ . However, we observed the strongest TE-polarized emission from the sidewalls with the far-field polar plot showing peaked intensity at  $\theta_{\text{inc}} = 21^\circ$ , which is three times greater than that from the corners. The emission from the sidewalls is associated with nearly TIR-confined open ray orbits for which only two of the bounces have  $\theta_{\text{inc}} < \theta_c$ . Selective pumping with a stripe-shaped pump beam and spectral analysis of the sidewall intensity provided more insight.

G. D. Chern and R. K. Chang acknowledge partial support to Yale University from the U.S. Air Force Office of Scientific Research (grant F33615-02-2-6066) and the Defense Advanced Research Projects Agency Semiconductor UV Optical Sources program under Space and Naval Warfare Systems Command (SPAWAR) Systems Center Contract N66001-02-C-8017. G. D. Chern's e-mail address is [grace.chern@yale.edu](mailto:grace.chern@yale.edu).

\*Present address, Hong Kong University of Science and Technology, Kowloon, Hong Kong.

## References

1. S. M. K. Thiyagarajan, D. A. Cohen, A. F. J. Levi, S. Ryu, R. Li, and P. D. Dapkus, *Electron. Lett.* **35**, 1253 (1999).
2. B. E. Little, J. S. Foresi, G. Steinmeyer, E. R. Thoen, S. T. Chu, H. A. Haus, E. P. Ippen, L. C. Kimerling, and W. Greene, *IEEE Photon. Technol. Lett.* **10**, 549 (1998).
3. A. W. Poon, F. Courvoisier, and R. K. Chang, *Opt. Lett.* **26**, 9 (2001).
4. H. Han, D. V. Forbes, and J. J. Coleman, *IEEE J. Quantum Electron.* **31**, 1994 (1995).
5. M. Born and E. Wolf, *Principles of Optics*, 7th ed. (Cambridge U. Press, Cambridge, 1999), Chap. 3 and App. VI.